Journal of Power Sources 430 (2019) 233–243

Contents lists available at ScienceDirect

Journal of Power Sources

journal homepage: www.elsevier.com/locate/jpowsour

# On-line fault diagnosis for proton exchange membrane fuel cells based on a fast electrochemical impedance spectroscopy measurement☆

Huaxin Lu, Jian Chen *, Chizhou Yan, Hao Liu

*The State Key Laboratory of Industrial Control Technology, College of Control Science and Engineering, Zhejiang University, Hangzhou, 310027, China*

ARTICLE INFO

*Keywords:*
Fault diagnosis
Proton exchange membrane fuel cells
Electrochemical impedance spectroscopy

ABSTRACT

In this paper, an on-line fault diagnosis method for proton exchange membrane fuel cells is proposed based on a fast electrochemical impedance spectroscopy measurement. Specifically, a fast electrochemical impedance spectroscopy measurement system is developed in order to reduce the measurement cost and time. The current pulse injection is used as the disturbance injection method, and the electrochemical impedance spectroscopy is obtained by the continuous wavelet transform and the maximum likelihood estimation. Then, the parameters of an improved equivalent circuit model are identified according to the electrochemical impedance spectroscopy, and three model parameters are selected as the features for fault diagnosis. On this basis, a multi-fault diagnosis algorithm is proposed based on the binary tree support vector machine classifier. Experimental results show that the proposed fault diagnosis method can realize accurate and fast on-line fault diagnosis for proton exchange membrane fuel cells.

## 1. Introduction

Proton exchange membrane fuel cells (PEMFCs) have the advantages of pollution-free, high efficiency, renewable fuel, high energy density, low noise, wide power range, refueling convenience, etc., and are considered to be one of the most promising power technologies [1,2]. Although many PEMFC projects are underway in the world, lifetime and cost are still the two major bottlenecks in the development of PEMFCs [3]. For many reasons, the actual lifetime of a PEMFC is much lower than the experimental lifetime provided by the manufacturer. Among them, the unavoidable faults such as fuel starvation and flooding in the actual operation are the important reasons leading to the drastic decrease of lifetime. The faults will lead to the serious degradation or even damage of PEMFC components, resulting in the performance degradation of PEMFCs [4]. Drying, flooding, and air starvation are the three most common faults that can reduce the performance and lifetime of PEMFCs [5]. Table 1 lists their causes and impacts on PEMFCs.

Accurate fault diagnosis not only can protect the PEMFCs, extend their lifetime, but also can greatly reduce the maintenance costs. Researchers have proposed many fault diagnosis methods for PEMFCs, such as the model-based, the machine learning-based, and the signal processing-based methods [10,11]. The model-based methods are implemented by establishing the PEMFC models using the complex mechanisms (electrochemistry, thermodynamics, electricity and fluidics) [11]. For the machine learning-based methods [12,13], the diagnosis process is considered as a black box, and the fault diagnosis is realized by using the machine learning algorithms. The signal processing-based methods tend to use the signal processing approaches such as the wavelet transform and the empirical mode decomposition to extract the features of monitoring data for fault detection and isolation [14]. However, most of these methods only use the monitoring data from the sensors of the PEMFC systems. Although they are simple to implement, the monitoring data can only reflect limited real state information within PEMFC stacks. Most of the time, faults occur locally, such as flooding and air starvation, which may not be evident in the monitoring data, leading to inaccurate diagnostic results. Therefore, the fault diagnosis needs to be based on the accurate internal state information. Electrochemical impedance spectroscopy (EIS)-based diagnosis is a kind of effective diagnosis methods that can obtain more information with additional measurement equipment. By injecting a small AC current as the disturbance signal to PEMFCs and measuring the response voltage, the EIS can be obtained from the two signals [15]. Since the EIS can provide abundant information such as the water content, the reactant concentration and the catalyst poisoning, which can accurately

☆ This work was supported by the National Natural Science Foundation of China (61433013).
* Corresponding author.
*E-mail address:* jchen@zju.edu.cn (J. Chen).

https://doi.org/10.1016/j.jpowsour.2019.05.028
Received 26 November 2018; Received in revised form 4 May 2019; Accepted 7 May 2019
Available online 21 May 2019

**Table 1**
Faults and their impacts on PEMFCs.

| Faults | Causes | Impacts on PEMFCs |
|---|---|---|
| Drying [5,6] | ● Insufficient level of gas humidification;<br>● High water removal rates;<br>● High cathode stoichiometry;<br>● Excessive stack temperature. | ● Dehydrating the membrane;<br>● Decreasing the membrane ionic conductivity;<br>● Increasing the activation polarization;<br>● Leading the irreversible membrane degradation. |
| Flooding [7,8] | ● Overload of humidity in the inlet gases;<br>● Inappropriate back pressure;<br>● Faults in water discharging;<br>● Low stack temperature;<br>● Higher current density. | ● Blocking the gas diffusion layer (GDL) and flow channel;<br>● Limiting the arrival rate of gaseous reactants;<br>● Reducing the PEMFCs performance;<br>● Accelerating the carbon corrosion. |
| Air starvation [6,9] | ● Faults in the air supply subsystem;<br>● Flooding is also a factor. | ● Reducing the reaction rate;<br>● Generation of hydrogen at cathode and oxygen at anode;<br>● Causing a reverse potential;<br>● Leading to an explosion. |

characterize the internal state of PEMFC stacks [16]. Moreover, unlike the model-based method, this method does not need to understand the complex operation mechanisms of PEMFCs and establish complex models. In practical applications, the mechanism model of PEMFCs can not take into account all situations, and is not suitable for on-line applications. Therefore, in this study, the EIS-based fault diagnosis method is adopted. A lot of researches have been done on the EIS-based methods. Existing EIS-based fault diagnosis methods can be roughly divided into two categories: The first type of method uses the geometric features of EIS curves to diagnose faults directly. The second type of method uses the equivalent circuit model (ECM) to fit EIS curves, and then uses the model parameters to diagnose faults. In Ref. [17], the experimental results showed that the drying, flooding, and anode catalyst poisoning faults had different effects on the shape of EIS curves. In Ref. [18], six geometric features were extracted and a fault diagnosis method based on fuzzy c-means clustering was proposed to diagnose the drying and flooding faults with different degrees. An improved Randles model was established in Ref. [19] and the effects of drying and flooding faults on the model parameters were analyzed. In Ref. [20], an ECM based fault diagnosis method was proposed for detecting the flooding, drying, and membrane deterioration faults of PEMFCs. In Ref. [4], the ECM was introduced as an auxiliary way to analyze the performance, consistency, and uniformity of PEMFC stacks.

Although there are many EIS-based fault diagnosis methods for PEMFCs, most of them are still in the stage of academic research. Few methods can be used in the practical applications due to the two main bottlenecks: (1) The time consumption of EIS measurement is too large (usually several minutes) [21]. (2) The EIS measurement equipment is usually expensive and bulky. Due to these two bottlenecks, most EIS-based fault diagnosis methods are used in the off-line applications, mainly used in laboratories. However, in the operation of PEMFCs, the ability to detect and isolate faults in time can greatly reduce the damage of PEMFCs and maintenance costs. Therefore, the on-line fault diagnosis is absolutely necessary for PEMFCs [22]. For the on-line fault diagnosis based on EIS, both the in-situ measurement and the quick diagnosis are required. On the one hand, the EIS can be measured while the system is working. On the other hand, the time consumption for the EIS measurement and fault diagnosis should be shortened to detect and isolate faults in time. In order to realize the on-line fault diagnosis, the both bottlenecks need to be addressed.

The long measurement time of EIS not only affects the time consumption of diagnosis, but also leads to the low frequency stability and nonlinear problems of EIS measurement [23]. To address this issue, various multi-frequency measurement methods have been proposed to shorten the measurement time. The authors of [24] proposed an EIS measurement approach based on perturbing PEMFCs with the chirp signal that contains a lot of frequencies. In Refs. [25,26], a multi-sine measurement technique was implemented, in which the PEMFCs were perturbed by the multi-sine signals rather than the single-sine signals. This is an excellent approach as it reduces the system disturbance at the same time. In Refs. [23,27], a Pseudo-Random Binary Sequence (PRBS) was utilized as the perturbation signal, and the measurement time is shortened to 60 s. However, these methods, while reducing the measurement time, are still a long process for on-line fault diagnosis of PEMFCs.

Nevertheless, how to inject disturbance signals into PEMFCs to implement the in-situ measurements remains a problem. Recent studies have shown that DC/DC converters can be used to achieve the disturbance injection. In Ref. [28], an on-line EIS measurement method integrated with a 6-phase interleaved boost converter was proposed by sending AC signals to the inductor current reference. In Refs. [29,30], a new approach for on-line impedance measurement was proposed by paralleling the DC/DC. Sinusoidal excitation signals were produced by controlling the output current of the converters. However, due to the bandwidth limitation of the converters, the frequency of excitation signals generated by the DC/DC converters is typically not high. Moreover, the dedicated converters also increase the cost and complexity of PEMFC systems. Another simple and practical method is the current pulse injection (CPI), which is widely used in battery testing [31]. This method has been proved to be effective in the impedance estimation of PEMFCs. In Ref. [32], a simple circuit consisting of a series resistor and a Metal Oxide Semiconductor Field Effect Transistor (MOSFET) was used to add the disturbance signal and a model-based method was proposed for the impedance estimation.

This paper proposes an on-line fault diagnosis method for PEMFCs based on a fast EIS measurement, which fills the gap between the academic research and the practical applications of EIS-based fault diagnosis. Firstly, a fast EIS measurement system is developed, where the maximum length sequence (MLS) disturbed current is injected into PEMFCs through a CPI circuit, and the EIS is obtained by the continuous wavelet transform and the maximum likelihood estimation. Secondly, an improved ECM is proposed to extract the EIS features. According to the selected features, an on-line fault diagnosis method based on the binary tree support vector machine (BT-SVM) classification algorithm is established to diagnose different faults. Finally, the effectiveness and accuracy of this method are validated by experiments. Faults considered in this paper include flooding, drying, and air starvation.

The contributions of this paper are summarized as follows:

1) An on-line PEMFC fault diagnosis method is proposed based on the fast EIS measurement. This method can effectively diagnose the faults in PEMFC stack such as the drying, flooding, and air starvation.
2) The MLS and continuous wavelet transform based impedance estimation algorithm greatly shorten the EIS measurement time. The CPI circuit provides a low cost, small-volume and effective solution for disturbance injection, demonstrating its commercial and engineering feasibility. With this method, the applications of the EIS technology can be greatly expanded.
3) For the EIS-based on-line fault diagnosis, a feature extraction method based on the improved ECM and the BT-SVM classifier is proposed. The experimental results demonstrate the feasibility and effectiveness of the proposed method.

The structure of this paper is organized as follows. In Section 2, the fault diagnosis problem is described and the proposed fault diagnosis method of PEMFCs is outlined. The fast EIS measurement system is developed in Section 3, and Section 4 presents the on-line fault diagnosis algorithm. Experimental verification and discussions are given in Section 5. Finally, Section 6 gives the conclusions.

## 2. On-line fault diagnosis method

### 2.1. Problem formulation

The work of this paper is based on the water-cooled PEMFC system with the structure shown in Fig. 1 (a). The PEMFC system is complex and the operation environment is harsh, which brings challenges to the ideal humidity management and fuel supply. Different types of faults such as flooding, drying, and air starvation can greatly affect the durability and reliability of PEMFCs. Therefore, the propose of this study is to propose an on-line method to diagnose different types of faults for PEMFCs.

### 2.2. Overview of on-line fault diagnosis method

As shown in Fig. 1 (b), the on-line fault diagnosis method consists of three steps, namely the current pulse injection, the impedance calculation, and the fault diagnosis.

***1) Current pulse injection:*** The CPI circuit is used to add a small AC component into the PEMFC current. In order to shorten the measurement time, the MLS with a large number of frequency components is selected as the excitation signal. Using the CPI circuit, the MLS current can be easily injected into the PEMFC stack. Then, the disturbance current and response voltage are sampled by the signal processing circuit and the data acquisition device.

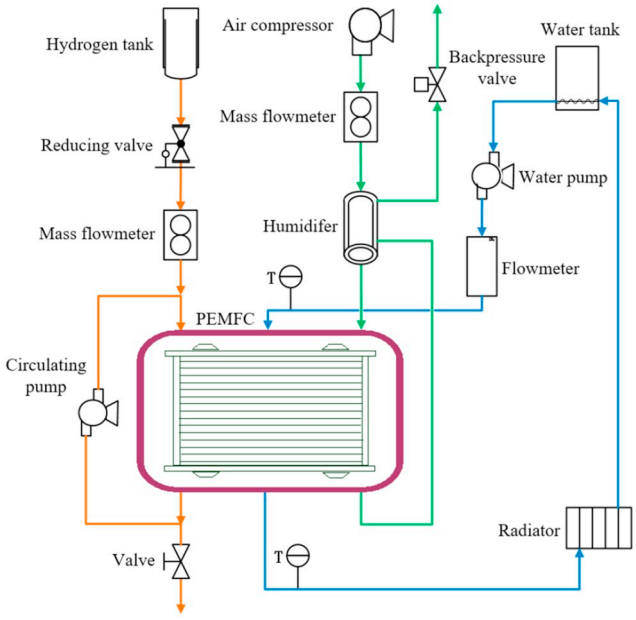


(a) Structure of the water-cooled PEMFC system.

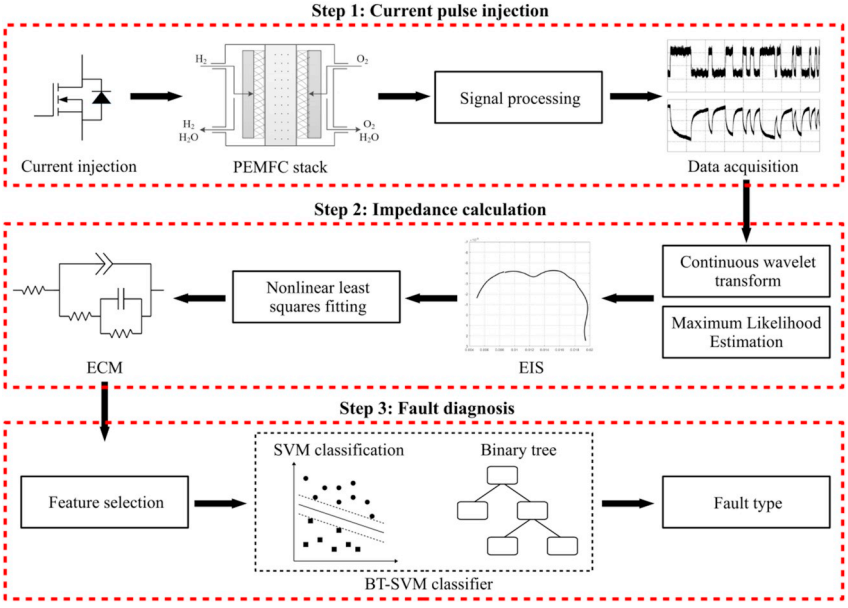


(b) On-line fault diagnosis diagram.

**Fig. 1.** The proposed on-line PEMFC fault diagnosis method.

***2) Impedance calculation:*** Based on the sampled voltage and current, the EIS is obtained by the continuous wavelet transform and the maximum likelihood estimation. Considering that the EIS has many redundant information, the ECM is utilized to describe the characteristics of EIS. The parameters of ECM are estimated by the nonlinear least square method.

***3) Fault diagnosis:*** In this step, the features for diagnosis are selected from the parameters of the ECM. With the selected features, the fault types are identified by the fault classifier based on the BT-SVM classification algorithm.

## 3. Fast EIS measurement system

Fig. 2 (a) shows the schematic of the fast EIS measurement system. The MLS signals are generated by a MLS generator and a digit-analog converter. Then, the MLS signals are injected into the PEMFC current through a parallel CPI circuit. In the measurement process, the current is sampled by a shunt resistance. The voltage and current of PEMFCs are measured by the signal processing circuit and the analog-digit converters. Finally, the data are transmitted to the host computer for further processing.

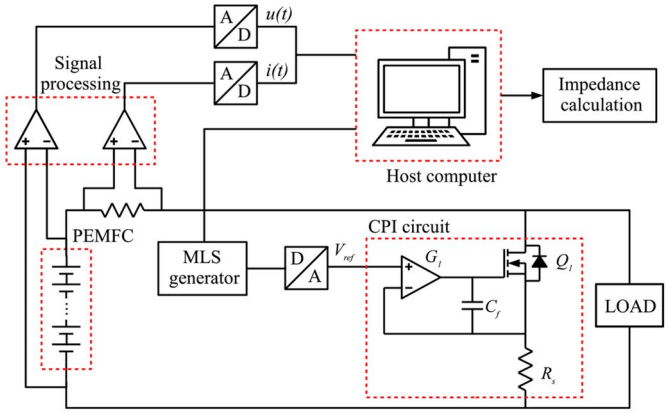


(a) Schematic of the fast EIS measurement system.

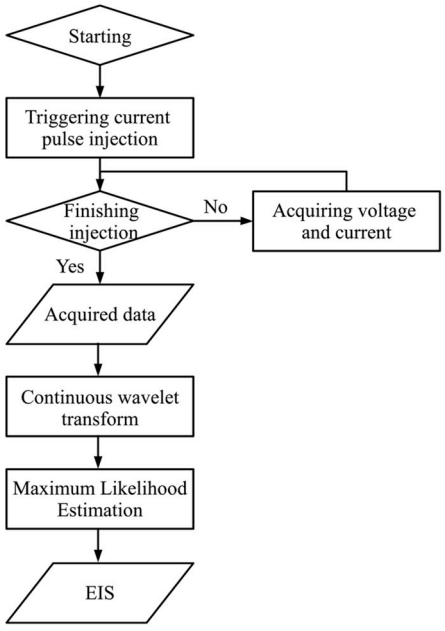


(b) Flow chart of the fast EIS measurement.

**Fig. 2.** Schematic and flowchart of the fast EIS measurement.

### 3.1. CPI circuit

The CPI circuit is implemented by a MOSFET in the feedback loop of an operational amplifier as shown in Fig. 2 (a). The MOSFET $Q_1$ works in the linear region and operates like a resistor. Thanks to a negative current feedback circuit composed of $G_1$ and the feedback resistance $R_s$, the current through $Q_1$ is constant. The compensation capacitance $C_f$ is utilized to improve the stability of $G_1$. Thanks to the characteristics of the operational amplifier, the disturbance current can be set by the voltage on the non-inverting input of $G_1$. By using a digit-analog converter, the disturbance current $I_{CPI}$ can be set by the reference voltage $V_{ref}$:

$$I_{CPI} = \frac{V_{ref}}{R_s}. \tag{1}$$

Then, the current pulse can be generated by setting the reference voltage alternately. The main advantage of the CPI circuit is that the high-frequency disturbance current can be easily injected by choosing the appropriate operational amplifier and the MOSFET. Moreover, compared with the CPI circuit implemented by a resistance and a MOSFET [32], the disturbance current in this circuit is controllable. Therefore, it can be used in different power conditions. Moreover, the circuit is low cost due to its simple architecture and fewer components.

### 3.2. MLS excitation signals

The MLS is a type of PRBS and has the white-noise-like properties in a wide frequency range [33]. Usually, the MLS signal can be generated by an $n$-stage digital shift register $a_i$ with the feedback coefficients $c_i$, which conforms to the linear recurrence [34]:

$$a_n = \left(\sum_{i=1}^{n} c_i a_i\right) mod(2). \tag{2}$$

For an $n$-bit MLS with a bit frequency of $f_s$, the power spectral density decreases less than $3dB$ in the frequency range of $[0, f_s/3]$. Besides, the distance of the spectral lines in the power spectrum is $\Delta f = f_s/(2^n - 1)$, which corresponds to the frequency resolution [33]. Therefore, the effective bandwidth of the MLS between $f_{min}$ and $f_{max}$ can be defined as:

$$f_{min} = \frac{f_s}{2^n - 1} \tag{3}$$

$$f_{max} = \frac{f_s}{3}.$$

Since the MLS disturbance current is adopted, it is necessary to determine the parameters of the signals such as the amplitude, the bit frequency, and the length. The selection of these parameters is based on two basic principles: shortening the injection time and improving the measurement accuracy.

The amplitude of disturbance current plays an important role in the EIS measurement. The excessive amplitude will lead to the operation point variation of PEMFCs due to the change of mass transport, while the too small amplitude will reduce the measurement accuracy [35]. Usually, an amplitude of 5% of the DC current is considered reasonable [15]. Moreover, in this work, the EIS is measured in the frequency band from 0.5 Hz to 500 Hz. Experiments show that when the frequency is less than 0.5 Hz, the low-frequency instability can lead to wrong results. When the frequency is higher than 500 Hz, the inductance at wires and electrical contacts will affect the measurement. Moreover, the EIS in this frequency band is able to provide enough information of PEMFCs. In order to meet the requirement of measuring bandwidth and reduce the time consumption, two MLS signals are used as the excitation signals. According to (3), the parameters of these two MLS signals are shown in

**Table 2**
Parameters of the MLS signals.

| $n$ | $f_s$ | Frequency band |
|---|---|---|
| 11 | 200 Hz | 0.5 Hz - 60 Hz |
| 13 | 1500 Hz | 60 Hz - 500 Hz |

Table 2.

With the parameters, the injection time of the excitation signals is:

$$T = \frac{2^{11}-1}{200} + \frac{2^{13}-1}{1500} \approx 16\ s. \tag{4}$$

During the MLS injection, the voltage and current of PEMFCs are sampled and recorded by the signal processing circuit and digit-analog converters. After injection, the collected data will be transmitted to the host computer for data processing and EIS calculation.

### 3.3. EIS estimation

For the traditional EIS measurements, the common method to calculate impedance is to calculate the Fourier transformation ratio of current and voltage signals [15]. However, the Fourier transform algorithm is not competent in this work because of the limitations of non-stable signal processing. Although the MLS signals have abundant frequency components, the components at each time are indeterminate, thus the time-frequency analysis is required. The continuous wavelet transform, as a common time-frequency analysis tool, has been widely used in many fields [36]. Recently, some studies have used the continuous wavelet transform to calculate impedance, and good results have been obtained [23,37]. For a continuous time signal function $f(t) \in L^2(R)$, the continuous wavelet transform is defined as [38]:

$$W_f(a,\tau) = \frac{1}{\sqrt{a}} \int_{-\infty}^{+\infty} f(t)\varphi\left(\frac{t-\tau}{a}\right) dt \tag{5}$$

where $W_f(a,\tau)$ is the wavelet coefficient with a scale parameter $a$ and a time parameter $\tau$, and $\varphi(t)$ is the mother wavelet. By choosing the different a and $\tau$, the mother wavelet shrinks, stretches and shifts in the time scale, and carries out the multi-resolution analysis. In this work, the Morlet Wavelet is chosen as the mother wavelet, which is defined as [38]:

$$\varphi(t) = \pi^{-\frac{1}{4}}\left(e^{-j\omega_0 t} - e^{-\frac{\omega_0^2}{2}}\right)e^{-\frac{t^2}{2}} \tag{6}$$

where $\omega_0$ is the central frequency of the wavelet which affects the time and frequency resolution.

Then, using the ratio of the wavelet coefficient of voltage and current at $a_0$, the impedance at scale $a_0$ with time variation is calculated [37]:

$$z(a_0,t) = \frac{u(a_0,t)}{i(a_0,t)} = \frac{W_u(a_0,t)}{W_i(a_0,t)}. \tag{7}$$

The result of (7) is a sequence of impedance at different time and the certain value of impedance needs to be estimated. According to Ref. [21], the wavelet coefficients of the voltage and the current at specific frequencies can be regarded as the zero-mean Gaussian circular complex random variables, and the probability density function of the impedance $z = z_r + jz_i$ is:

$$f(z_r,z_i) = \frac{1-|\rho|^2}{\pi\sigma_u^2\sigma_i^2}\left(\frac{|z|^2}{\sigma_u^2} + \frac{1}{\sigma_i^2} - 2\frac{\rho_r z_r - \rho_i z_i}{\sigma_u\sigma_i}\right)^{-2} \tag{8}$$

where $z_r$ and $z_i$ are the real and imaginary parts of the impedance $z$. $\sigma_u^2$ and $\sigma_i^2$ are the variances of wavelet coefficients of voltage and current, respectively. $\rho = \rho_r + j\rho_i$ is the complex correlation coefficient which can be calculate by the correlation matrix [39]:

$$\begin{bmatrix} \sigma_u^2 & \rho\sigma_u\sigma_i \\ \rho^*\sigma_u\sigma_i & \sigma_i^2 \end{bmatrix} = \begin{bmatrix} E[W_u(a_0,t)W_u(a_0,t)^*] & E[W_u(a_0,t)W_i(a_0,t)^*] \\ E[W_i(a_0,t)W_u(a_0,t)^*] & E[W_i(a_0,t)W_i(a_0,t)^*] \end{bmatrix}. \tag{9}$$

Then the impedance can be obtained by the maximum likelihood estimation:

$$z = \arg\max_z f(z_r,z_i) \tag{10}$$

In summary, the principle of impedance estimation algorithm is as follows: Firstly, the frequency information of the MLS disturbance current and response voltage signals is extracted by the continuous wavelet transform and stored in the wavelet coefficients. Secondly, the probability density function of PEMFC impedance is obtained by the particular distribution of the wavelet coefficients. Thirdly, the maximum likelihood estimation is utilized to obtain the optimal impedance estimation from the probability density function. Finally, the EIS can be obtained by calculating the impedance at different frequencies. Fig. 2 (b) shows the detailed flow chart of EIS measurement. When the measurement begins, the CPI circuit is generated and the MLS disturbance current is produced and injected to PEMFCs. At the same time, the voltage and current are collected and saved. After injection, the EIS is obtained by the continuous wavelet transform and the maximum likelihood estimation.

## 4. Fault diagnosis algorithm design

After the EIS measurement is completed, it is necessary to continue to study how to use the measured EIS to realize the fault diagnosis of PEMFCs. The block diagram of the proposed fault diagnosis algorithm is shown in Fig. 3, including the on-line and the off-line stages. In the off-line stage, the training dataset is obtained through the fault experiments. Then, the diagnostic features are extracted and selected according to the training dataset. After that, the fault classifier is designed by choosing the classification algorithm and formulating the diagnosis rules. Finally, the training dataset is utilized to train the fault classifier. In the on-line stage, the real-time data are recorded in the on-line operation process. Using the features extracted from EIS, the trained classifier can identify the specific fault types.

The feature selection and the classification algorithms are two

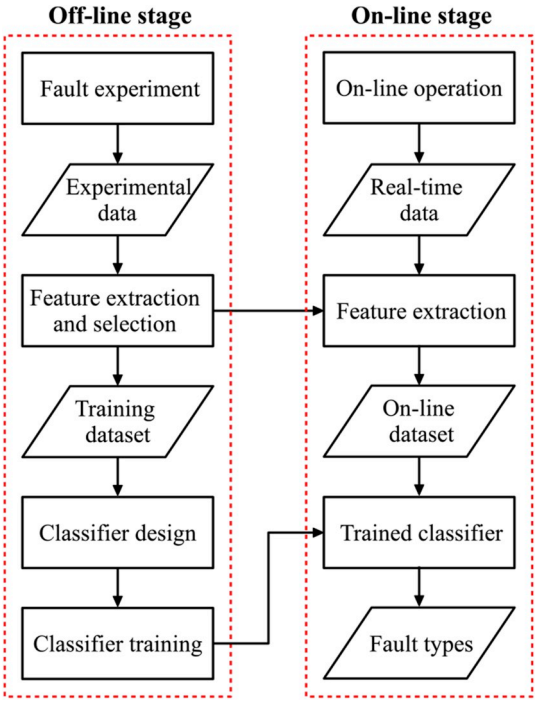


**Fig. 3.** Diagram of the fault diagnosis process.

essential parts of the fault diagnosis algorithm that mainly affect the accuracy and sensitivity of diagnosis. In this section, the ECM based feature extraction method and the BT-SVM based classification algorithm are proposed.

### 4.1. Feature extraction and selection

Generally, two methods are usually utilized to extract the features from EIS: (1) The geometric features of EIS are extracted directly. (2) Fitting EIS with the ECM, then extracting the model parameters as the features. Although the first method is intuitive and simple, the biggest shortcoming is that only part of the impedance information is used. Abnormal features can sometimes occur due to the local irregularity of the spectral lines. Therefore, it is usually necessary to use both the smoothing algorithm and the outlier removal. For the second method, all the impedance information can be used in the model fitting process to make the diagnosis more accurate and robust.

The Randles ECM [40] is one of the most common and practical ECM. As shown in Fig. 4 (a), this ECM consists of four elements: $R_m$, $R_p$, $Z_w$, and $C_{dl}$. The ohmic resistance $R_m$ represents for the internal resistance of PEMFCs. The polarization resistance $R_p$ characterizes the oxygen reduction reaction. The double-layer capacitance introduced by the electrodes is represented by $C_{dl}$. The finite-length Warburg impedance $Z_w$ represents the limitation of mass transfer [10].

In this study, an improved ECM is established to simplify the Randles ECM and improve the fitting accuracy as show in Fig. 4 (b). Firstly, too many parameters and the complex analytical expression in the Warburg impedance make the Randles ECM more difficult for on-line EIS fitting and analysis. Besides, for ECM, it is better to use circuit elements such as resistance, capacitance and inductance to model, which can directly reflect the impact of various electrochemical processes on impedance. Some researches have proposed that the Warburg impedance can be replaced by the RC circuit [41]. In this study, $Z_w$ in Fig. 4 (a) is approximately replaced by parallel $R_w$ and $C_w$ in Fig. 4 (b). Moreover, unlike some of other electrochemical systems such as the battery, PEMFCs have porous electrodes, which can improve the adsorption capacity of the reactant gas. Therefore, the double-layer capacitor cannot well represent the electrodes of PEMFCs. According to Ref. [15], the distribution parameters caused by the porous electrodes can be expressed by the constant phase element (CPE) in Fig. 4 (b) instead of the $C_{dl}$ in Fig. 4 (a). The impedance of CPE is expressed as:

$$Z_{CPE} = \frac{1}{Q(j\omega)^n} \tag{11}$$

where $n$ is the CPE exponent representing the distribution parameters of the electrodes, $Q$ is the pseudo-capacitance. Then, the impedance of the improved ECM can be calculated as follows:

$$Z = R_m + \frac{1}{Q(j\omega)^n + \frac{1}{R_p + \frac{1}{j\omega C_w + \frac{1}{R_w}}}}. \tag{12}$$

The parameters in (12) can be estimated by the EIS. In order to make full use of all the EIS information, the nonlinear least square method is adopted in this study [42].

There are five components in the improved ECM. Among them, the CPE is determined by the physical characteristics of the electrodes, and is hardly affected by the operating conditions. Moreover, considering that the mass transfer process mainly affects the low frequency part of EIS, $R_w$ is more representative of mass transfer process than $C_w$. Therefore, $R_m$, $R_p$, and $R_w$ are selected as the features for fault classification, which are mainly affected by the membrane resistance, the charge transfer, and the mass transfer.

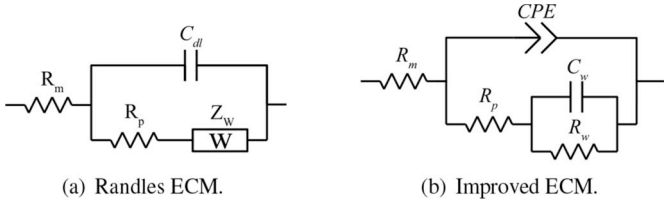


(a) Randles ECM. (b) Improved ECM.

**Fig. 4.** ECMs of PEMFCs.

### 4.2. Fault classifier

In actual operation, PEMFCs mostly work under the normal condition. In contrast, the durations of the fault states are relatively short. Therefore, the diagnosis algorithm needs to satisfy the requirement of less training data in order to get accurate diagnosis results. In this case, SVM algorithm is a suitable classification algorithm that can get good generalization even if the amount of training data is small [43]. Moreover, SVM algorithm also has small storage space and high computational efficiency as it uses the support vectors composed of training data subsets for classification [44].

The SVM algorithm was originally developed for binary classification. Actually, many faults can occur in PEMFCs, such as flooding, drying, and air starvation. In order to achieve accurate fault diagnosis, a multi-state classification problem needs to be solved. BT-SVM can achieve high computational speed and classification efficiency for multi-state classification tasks [45]. In this study, the BT-SVM based fault classifier is designed as shown in Fig. 5, which includes a binary tree with four SVM classifiers, namely the pre-classifier, the drying classifier, the flooding classifier, and the air starvation classifier. Firstly, the pre-classifier is utilized to judge whether the PEMFCs are in the normal state. This is a fast way to determine whether a fault occurs. Then, if the classification result of the pre-classifier is the fault state, the drying classifier will determine whether the PEMFCs are in the drying fault state. Then, the flooding fault can be diagnosed by the flooding classifier and the air starvation fault can be diagnosed by the air starvation classifier.

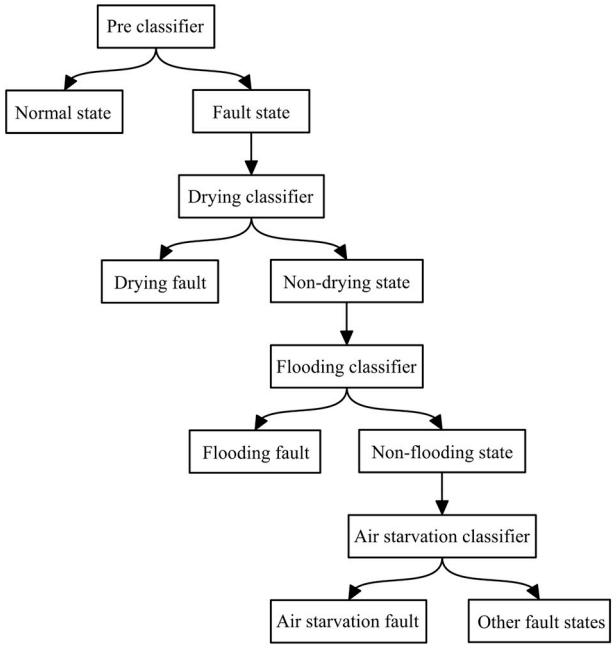


**Fig. 5.** BT-SVM based fault classifier.

## 5. Experimental results and discussions

### 5.1. Experimental platform

The experiments are carried out on a 3 kW PEMFC experimental platform, as shown in Fig. 6. The composition of the platform is described as follows [2]:

***1) PEMFC system:*** The structure of the PEMFC system is shown in Fig. 1 (a). The core of this system is a 3 kW PEMFC stack made by Sunrise Power Inc., which consists of 18 single cells. In the cathode of the system, the high pressure air is maintained by a vane compressor from VAIREX and humidified by a gas-to-gas humidifier with the model FC – 300. For the anode, the hydrogen is supplied by a hydrogen tank. A reducing valve from TESCOM is used to control the pressure at the anode inlet. Due to the circulating pump, the utilization rate of hydrogen is improved. During the operation of the system, the produced water and the nitrogen permeated from the cathode are expelled periodically through a purge valve. In addition, the temperature of the PEMFC stack is controlled by the cooling water circulated by the water pump. Moreover, some sensors, such as the pressure sensors from Noshok and the thermocouples from OMRON, are used for the system monitoring and controlling. Table 3 summarizes the normal operation parameters of the system.

***2) Electronic load:*** As shown in Fig. 6 (a), the output power of the PEMFC stack is set by a DC electronic load from TDI Power.

***3) Control unit:*** The platform is controlled and monitored by a real-time data processor from National Instruments as shown in Fig. 6 (a), the model is PXIe-1065. The control program developed by LABVIEW software runs on the host computer to maintain the ideal performance of the platform. All experimental data can be obtained and saved with a sampling time of 0.01 s.

***4) EIS measurement system:*** Fig. 6 (b) shows the fast EIS measurement system. The CPI circuit controlled by a STM32F103 microcontroller is in paralleled with the PEMFC stack for disturbance injection. A shunt resistor is connected in series with the PEMFC stack to sample the output current. In the signal processing circuit, the voltage of PEMFC stack and the shunt resistance is processed and sampled by the high-speed data acquisition (DAQ) device. The total size of the equipment in Fig. 6 (b) is $30cm \times 25cm \times 8cm$, which is much smaller than the traditional EIS measurement equipment. In addition, a host computer with Intel i5-4200 M CPU and 8 GB RAM is connected to receive the sampling data from the DAQ device and send commands to the microcontroller. Some operating parameters of the system are shown in Table 4.

**Table 3**
Normal operation conditions of the PEMFC system.

| Conditions | Value |
|---|---|
| Current | 150 A |
| Voltage | 12.5 V |
| Air stoichiometry | 2.5 |
| Inlet pressure of anode | 7 psi |
| Inlet pressure of cathode | 5 psi |
| Dew point of anode | 42 °C |
| Dew point of cathode | 60 °C |
| Operating temperature | 65 °C |
| Purge interval | 40 s |
| Purge duration | 0.5 s |

During the measurement, the host computer first sends the startup instruction to the microcontroller. The digital-analog converter of the microcontroller them generates reference voltage signals to control the CPI circuit for injecting the two MLS signals described in Table 2. The voltage and current are converted into standard signals by the signal processing circuit and collected by the high speed data acquisition (DAQ) device. After that, the data are sent to the host computer through the USB interface for EIS estimation. Fig. 7 (a) and Fig. 7 (b) show the current and voltage during the injection, where the load current is 150 A and the perturbed current is set to 7.5 A.

The experimental program in the host computer is developed by C++ and MATLAB. During the experiment, the program triggers the microcontroller to inject the disturbance current, estimates the EIS, and outputs the fault diagnosis results. Fig. 7 (c) shows a result of EIS estimation. The red part of the EIS curve is estimated by the high-frequency excitation signal and the blue part is estimated by the low-frequency excitation signal. The time consumption for the EIS estimation and the

**Table 4**
Operating parameters of the EIS measurement system.

| Parameters | Value |
|---|---|
| Maximum current pulse | 10 A |
| Shunt resistance | 200 A/75 mV |
| Bandwidth of signal processing circuit | 20 kHz |
| Sample Rate of DAQ device | 50 kHz |
| Resolution of DAQ device | 16 bit |

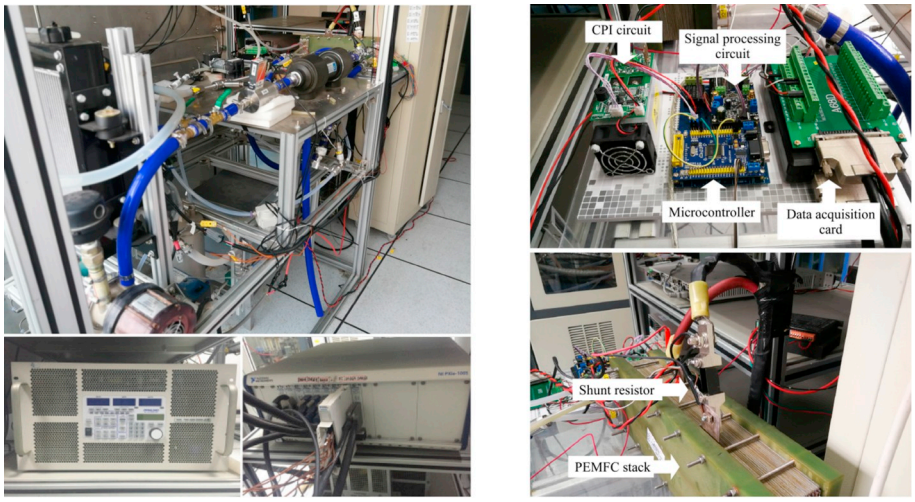


(a) PEMFC system, electric load, and PIX platform. (b) Fast EIS measurement system.

**Fig. 6.** Experimental platform.

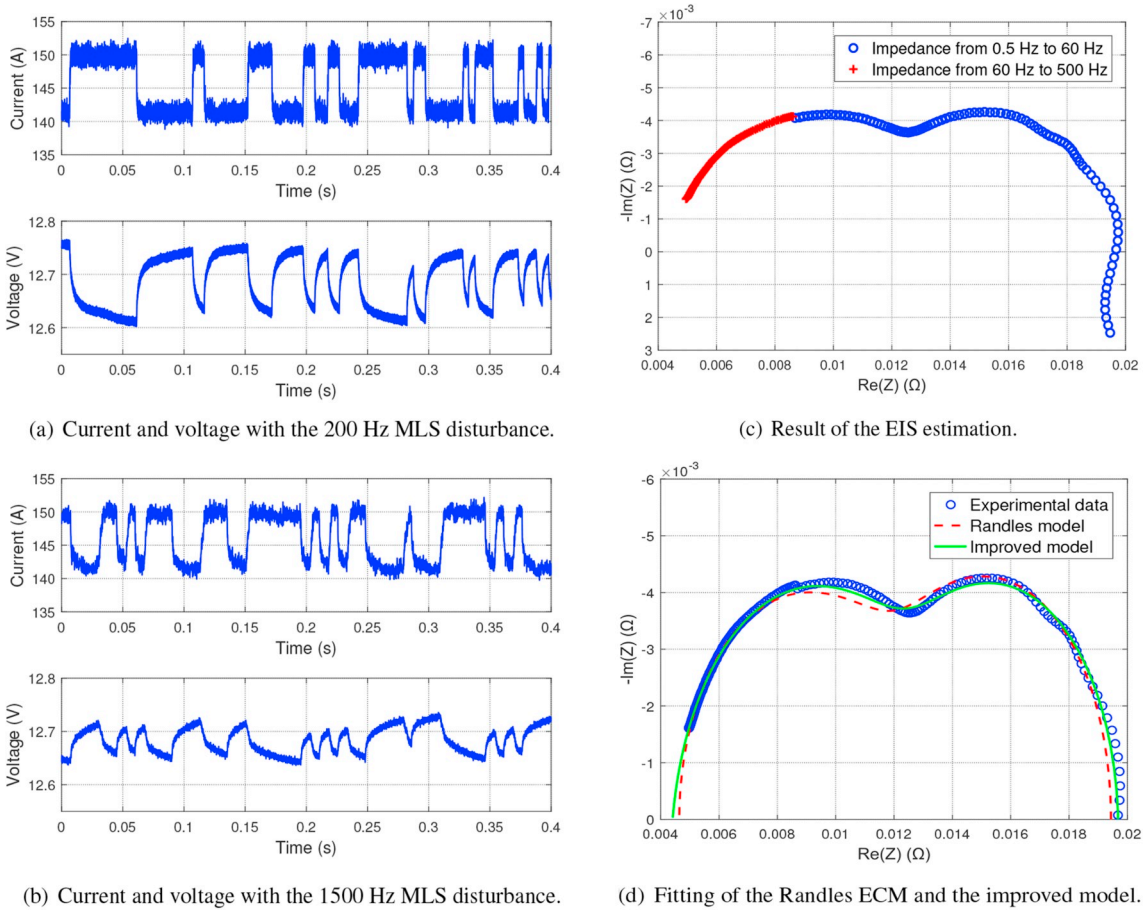


(a) Current and voltage with the 200 Hz MLS disturbance.

(c) Result of the EIS estimation.

(b) Current and voltage with the 1500 Hz MLS disturbance.

(d) Fitting of the Randles ECM and the improved model.

**Fig. 7.** Test results of the fast EIS measurement system.

fault diagnosis is about 18 s. Therefore, the whole time for the disturbance injection, the EIS measurement, and the fault diagnosis is about 34 s.

To verify the accuracy of the improved ECM, the fittings of the two ECMs in Fig. 4 are shown in Fig. 7 (d). The accuracy indexes of the two ECMs are shown in Table 5, including the mean square error (MSE) and the mean relative error (MRE). Their calculation formulas are as follows:

$$MSE = \frac{1}{n}\sum_{i=1}^{n}\left(\widehat{y}_i - y_i\right)^2$$
$$MRE = \frac{1}{n}\sum_{i=1}^{n}\left|\frac{\widehat{y}_i - y_i}{y_i}\right| \quad (13)$$

where $n$ is the sampling number, $y_i$ and $\widehat{y}_i$ are the experimental data and the result fitted by the ECM, respectively.

As depicted in Fig. 7 (d) and Table 5, the improved ECM has a better fitting accuracy than the Randles ECM. Specifically, in the low frequency region (the right side of the curve), the fitting accuracy of the two ECMs is similar, which shows that the Warburg impedance can be well replaced by $R_w$ and $C_w$. In addition, near the transition point between the two semicircles, the improved ECM can predict the direction of the curve more accurately due to the use of CPE. In conclusion, the improved ECM is simple and accurate, and it is an ideal on-line EIS analysis ECM.

**Table 5**
Accuracy indexes of the two models.

| Models | MSE | MRE |
|---|---|---|
| Randles ECM | $2.264 \times 10^{-7}$ | 0.0359 |
| Improved ECM | $2.158 \times 10^{-7}$ | 0.0283 |

### 5.2. Fault analysis and off-line training

Based on the experimental platform, the fault experiments are designed to analyze the faults and get the training data. The faults are generated by changing the operational conditions of the PEMFC system. All the PEMFC states considered include the normal state and the three fault states: drying, flooding, and air starvation. The operations in different states are shown in Table 6. In order to guarantee the accuracy, other operating conditions are maintained as the values in Table 3. During the experiment, 74 EIS curves in four states were measured and recorded, including 28 EIS curves in the normal state, 19 EIS curves in the drying fault state, 11 EIS curves in the flooding fault state, and 16 EIS curves in the air starvation fault state. Four typical EIS measurements in four different states with the ECM fitting curves are shown in Fig. 8 (a).

In order to analyze the influence of different states on the parameters of the ECM, the average values of the three selected parameters $R_m$, $R_p$, and $R_w$ (Fig. 4 (b)) in each state are listed in Table 7. The ohmic resistance $R_m$ increases obviously in the drying state and does not change much in other states. The polarization resistance $R_p$ increases in all three

**Table 6**
Operations with different states.

| PEMFC states | Operations |
|---|---|
| Normal | Normal operation |
| Drying fault | Supply dry air, set the purge interval to 20 s, and set the purge duration to 2 s to accelerate the water moving out |
| Flooding fault | Stop the circulating pump and purge valve to prevent the water moving out |
| Air starvation fault | Set the cathode stoichiometry to 1.6 by the air compressor |

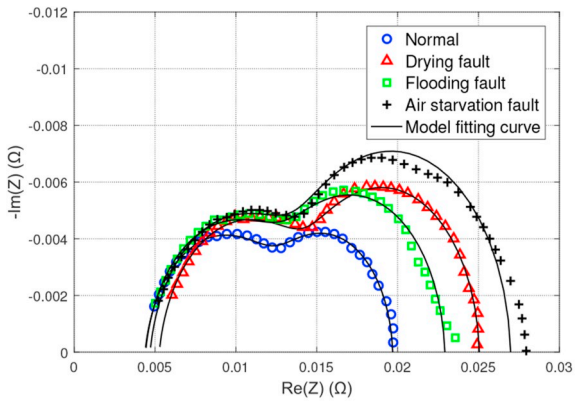


(a) Typical EIS and model fitting curves for different states.

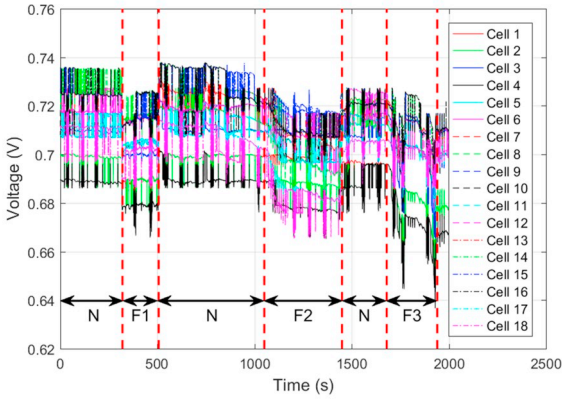


(b) The voltage of single cells during the experiment.

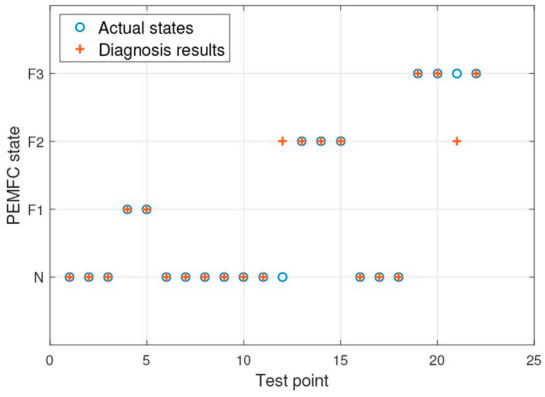


(c) On-line experimental results.

**Fig. 8.** Experimental results.

fault states. For the Warburg resistance $R_w$, it has similar effects. But $R_w$ in the air starvation state is larger than it in the other two fault states. Through the analysis of these features, it is proved that the parameters of the ECM have different characteristics in different states, and these three parameters can be used as the reliable features for fault diagnosis of PEMFCs.

**Table 7**
Average of selected parameters in different states.

| PEMFC states | $R_m$ ($m\Omega$) | $R_p$ ($m\Omega$) | $R_w$ ($m\Omega$) |
|---|---|---|---|
| Normal | 4.437 | 9.588 | 6.114 |
| Drying fault | 5.176 | 10.462 | 8.447 |
| Flooding fault | 4.565 | 10.916 | 8.193 |
| Air starvation fault | 4.527 | 10.921 | 12.284 |

**Table 8**
Training results.

| States | Correct result | Incorrect result | Accuracy rate |
|---|---|---|---|
| Normal | 28 | 0 | 100% |
| Drying fault | 19 | 1 | 95% |
| Flooding fault | 11 | 0 | 100% |
| Air starvation fault | 16 | 0 | 100% |

Based on the training data obtained, the fault classifier shown in Fig. 5 is trained off-line. The training results are shown in Table 8. For the training dataset, the average classification accuracy is 98.65%.

### 5.3. On-line validation

The on-line validation experiment is designed to evaluate the performance of the proposed fault diagnosis method. The experimental process is shown in Table 9. Three types of faults occur in turn, and the normal states between the two fault states are set to recover the PEMFC stack from the fault states. During the experiment, the fault diagnosis program runs every 80 s, and there are 22 diagnoses. Fig. 8 (b) shows the variations of single cell voltages during the experiment.

The actual states and diagnosis results are shown in Fig. 8 (c). It can be seen that most of the results are correct except for two missed diagnoses. For the first missed diagnosis, the EIS is obtained at the critical state that the drying fault is created. In this study, the determination of the drying state is based on the significant voltage drop, because the humidity of the membrane is difficult to obtain in real time. At this state, although the cell voltages do not decrease significantly, the water content of the membrane is already lower than the rated value. Therefore, this is not a true missed diagnosis. For the second missed diagnosis, there is a serious performance degradation in PEMFC stack due to the long time fault experiments (although the recovery time is set between the faults, it is not enough to fully recover the PEMFC). Therefore, in this case, the fault classifier cannot diagnose the state of the PEMFC stack well. In addition, in the actual operation process, this phenomenon of multiple faults occurring continuously is almost impossible to exist. In this paper, the fault is designed in this way only for the convenience of testing the proposed fault method.

In conclusion, the on-line experimental results show that the proposed method is suitable for on-line fault diagnosis of PEMFCs. Firstly, the PEMFC is perturbed by the MLS signals, which makes the measurement time much shorter than the traditional method, thus realizing fast fault diagnosis. Secondly, although the three faults can cause similar voltage drop in the experiment, they can be well diagnosed by the selected features. The BT-SVM classifier provides a fast and high-precision way for on-line fault diagnosis. Although there are some outliers in the EIS measurements, the classification results are still accurate due to the robustness of the ECM based feature extraction. Furthermore, it is also feasible to extend this method to other PEMFC faults by retraining the BT-SVM classifier.

**Table 9**
On-line experimental process.

| Start Time (s) | Stop Time (s) | Setting state | Samples |
|---|---|---|---|
| 0 | 320 | Normal (N) | 3 |
| 320 | 506 | Air starvation fault (F1) | 2 |
| 506 | 1050 | Normal (N) | 7 |
| 1050 | 1450 | Drying fault (F2) | 3 |
| 1450 | 1680 | Normal (N) | 3 |
| 1680 | 1940 | Flooding fault (F3) | 4 |

## 6. Conclusions

In this paper, an on-line PEMFC fault diagnosis method is proposed based on a fast EIS measurement. First of all, the fast EIS measurement system is developed. The CPI circuit is utilized to inject the double MLS disturbing signals into the PEMFC stacks and the EIS is obtained by the continuous wavelet transform and maximum likelihood estimation. In this way, the time for EIS measurement can be shortened to 34 s, making on-line applications feasible. At the same time, the cost and size of the developed system are also lower than most of conventional EIS equipment. There is no doubt that the developed system can meet the size requirements of most PEMFC applications. Then, based on the improved ECM, the features for diagnosis are extracted from the obtained EIS. After that, an on-line fault diagnosis algorithm based on the BT-SVM algorithm is developed to detect different faults by using the selected features. Finally, experimental results show that the proposed method has short diagnostic period and high accuracy in the flooding, drying, and air starvation faults diagnosis, which verifies the good performance of the proposed fault diagnosis method for PEMFCs.

There are also limitations of this method. Firstly, the complexity of the EIS estimation algorithm is fairly high, thus the computing equipment with high performance is required. Secondly, using the CPI circuit, this method will consume slight power to inject the disturbing current to PEMFCs, which can reduce the efficiency of PEMFC systems. Thirdly, some experiments are still needed to obtain the training data when the method is applied to a new PEMFC system. Based on these limitations, our future work will mainly focus on improving the method and making the method more suitable for practical applications.

## References


[1] O.Z. Sharaf, M.F. Orhan, An overview of fuel cell technology: fundamentals and applications, Renew. Sustain. Energy Rev. 32 (2014) 810–853, https://doi.org/10.1016/j.rser.2014.01.012.

[2] J. Chen, Z. Liu, F. Wang, Q. Ouyang, H. Su, Optimal oxygen excess ratio control for PEM fuel cells, IEEE Trans. Control Syst. Technol. 26 (5) (2018) 1711–1721, https://doi.org/10.1109/TCST.2017.2723343.

[3] A. Alaswad, A. Baroutaji, H. Achour, J. Carton, A.A. Makky, A. Olabi, Developments in fuel cell technologies in the transport sector, Int. J. Hydrogen Energy 41 (37) (2016) 16499–16508, https://doi.org/10.1016/j.ijhydene.2016.03.164.

[4] Z. Hu, L. Xu, J. Li, Q. Gan, X. Xu, Z. Song, Y. Shao, M. Ouyang, A novel diagnostic methodology for fuel cell stack health: performance, consistency and uniformity, Energy Convers. Manag. 185 (2019) 611–621, https://doi.org/10.1016/j.enconman.2019.02.031.

[5] R. Lin, X. Xi, P. Wang, B. Wu, S. Tian, Review on hydrogen fuel cell condition monitoring and prediction methods, Int. J. Hydrogen Energy 44 (11) (2019) 5488–5498, https://doi.org/10.1016/j.ijhydene.2018.09.085.

[6] H. Chen, X. Zhao, T. Zhang, P. Pei, The reactant starvation of the proton exchange membrane fuel cells for vehicular applications: a review, Energy Convers. Manag. 182 (2019) 282–298, https://doi.org/10.1016/j.enconman.2018.12.049.

[7] P. Pei, Y. Li, H. Xu, Z. Wu, A review on water fault diagnosis of PEMFC associated with the pressure drop, Appl. Energy 173 (2016) 366–385, https://doi.org/10.1016/j.apenergy.2016.04.064.

[8] D.G. Sanchez, P.L. Garcia-Ybarra, PEMFC operation failure under severe dehydration, Int. J. Hydrogen Energy 37 (8) (2012) 7279–7288, https://doi.org/10.1016/j.ijhydene.2011.11.059.

[9] D. Ko, Y. Kang, J. Yang, J. Jeong, G. Choi, D. Kim, Polarization characteristics and property distributions of a proton exchange membrane fuel cell under cathode starvation conditions, Int. J. Energy Res. 34 (2010) 865–877, https://doi.org/10.1002/er.1603.

[10] R. Petrone, Z. Zheng, D. Hissel, M. Pera, C. Pianese, M. Sorrentino, M. Becherif, N. Yousfi-Steiner, A review on model-based diagnosis methodologies for PEMFCs, Int. J. Hydrogen Energy 38 (17) (2013) 7077–7091, https://doi.org/10.1016/j.ijhydene.2013.03.106.

[11] A. Benmouna, M. Becherif, D. Depernet, F. Gustin, H. Ramadan, S. Fukuhara, Fault diagnosis methods for proton exchange membrane fuel cell system, Int. J. Hydrogen Energy 42 (2) (2017) 1534–1543, https://doi.org/10.1016/j.ijhydene.2016.07.181.

[12] J. Liu, Q. Li, W. Chen, T. Cao, A discrete hidden markov model fault diagnosis strategy based on k-means clustering dedicated to PEM fuel cell systems of tramways, Int. J. Hydrogen Energy 43 (27) (2018) 12428–12441, https://doi.org/10.1016/j.ijhydene.2018.04.163.

[13] T. Sutharssan, D. Montalvao, Y. Chen, W. Wang, C. Pisac, H. Elemara, A review on prognostics and health monitoring of proton exchange membrane fuel cell, Renew. Sustain. Energy Rev. 75 (2017) 440–450, https://doi.org/10.1016/j.rser.2016.11.009.

[14] M. Ibrahim, U. Antoni, N.Y. Steiner, S. Jemei, C. Kokonendji, B. Ludwig, P. Mooteguy, D. Hissel, Signal-based diagnostics by wavelet transform for proton exchange membrane fuel cell, Energy Procedia 74 (2015) 1508–1516, https://doi.org/10.1016/j.egypro.2015.07.708.

[15] X. Yuan, H. Wang, J.C. Sun, J. Zhang, AC impedance technique in PEM fuel cell diagnosisa review, Int. J. Hydrogen Energy 32 (17) (2007) 4365–4380, https://doi.org/10.1016/j.ijhydene.2007.05.036.

[16] W. Merida, D.A. Harrington, J.M.L. Canut, G. McLean, Characterisation of proton exchange membrane fuel cell (PEMFC) failures via electrochemical impedance spectroscopy, J. Power Sources 161 (1) (2006) 264–274, https://doi.org/10.1016/j.jpowsour.2006.03.067.

[17] J.M.L. Canut, R.M. Abouatallah, D.A. Harrington, Detection of membrane drying, fuel cell flooding, and anode catalyst poisoning on pemfc stacks by electrochemical impedance spectroscopy, J. Electrochem. Soc. 153 (5) (2006), https://doi.org/10.1149/1.2179200. A857–A864.

[18] Z. Zheng, M.C. Pera, D. Hissel, M. Becherif, K.S. Agbli, Y. Li, A double-fuzzy diagnostic methodology dedicated to online fault diagnosis of proton exchange membrane fuel cell stacks, J. Power Sources 271 (2014) 570–581, https://doi.org/10.1016/j.jpowsour.2014.07.157.

[19] N. Fouquet, C. Doulet, C. Nouillant, G. Dauphin-Tanguy, B. Ould-Bouamama, Model based PEM fuel cell state-of-health monitoring via ac impedance measurements, J. Power Sources 159 (2) (2006) 905–913, https://doi.org/10.1016/j.jpowsour.2005.11.035.

[20] A. Hernandez, D. Hissel, R. Outbib, Modeling and fault diagnosis of a polymer electrolyte fuel cell using electrical equivalent analysis, IEEE Trans. Energy Convers. 25 (1) (2010) 148–160, https://doi.org/10.1109/TEC.2009.2016121.

[21] A. Debenjak, J. Petrovi, P. Bokoski, B. Musizza, ani Jurii, Fuel cell condition monitoring system based on interconnected DC-DC converter and voltage monitor, IEEE Trans. Ind. Electron. 62 (8) (2015) 5293–5305, https://doi.org/10.1109/TIE.2015.2434792.

[22] J. Liu, Q. Li, W. Chen, Y. Yan, X. Wang, A fast fault diagnosis method of the pemfc system based on extreme learning machine and dempster-shafer evidence theory, IEEE Trans. Transport. Electrification 5 (1) (2018) 271–284, https://doi.org/10.1109/TTE.2018.2886153.

[23] A. Debenjak, P. Bokoski, B. Musizza, J. Petrovi, ani Jurii, Fast measurement of proton exchange membrane fuel cell impedance based on pseudo-random binary sequence perturbation signals and continuous wavelet transform, J. Power Sources 254 (2014) 112–118, https://doi.org/10.1016/j.jpowsour.2013.12.094.

[24] L. Das, B. Srinivasan, R. Rengaswamy, On-line performance monitoring of PEM fuel cell using a fast EIS approach, in: American Control Conference, Chicago, IL, USA, 2015, pp. 1611–1616, https://doi.org/10.1109/ACC.2015.7170963.

[25] C. Brunetto, A. Moschetto, G. Tina, PEM fuel cell testing by electrochemical impedance spectroscopy, Electr. Power Syst. Res. 79 (1) (2009) 17–26, https://doi.org/10.1016/j.epsr.2008.05.012.

[26] N. Katayama, S. Kogoshi, Real-time electrochemical impedance diagnosis for fuel cells using a DC-DC converter, IEEE Trans. Energy Convers. 30 (2) (2015) 707–713, https://doi.org/10.1109/TEC.2014.2376529.

[27] P. Manganiello, G. Petrone, M. Giannattasio, E. Monmasson, G. Spagnuolo, FPGA implementation of the EIS technique for the on-line diagnosis of fuel-cell systems, in: IEEE International Symposium on Industrial Electronics, Edinburgh, UK, 2018, pp. 981–986, https://doi.org/10.1109/ISIE.2017.8001379.

[28] H. Wang, A. Gaillard, D. Hissel, Online electrochemical impedance spectroscopy detection integrated with step-up converter for fuel cell electric vehicle, Int. J. Hydrogen Energy 44 (2) (2019) 1110–1121, https://doi.org/10.1016/j.ijhydene.2018.10.242.

[29] P. Hong, J. Li, L. Xu, M. Ouyang, C. Fang, Modeling and simulation of parallel DC/DC converters for online AC impedance estimation of PEM fuel cell stack, Int. J. Hydrogen Energy 41 (4) (2016) 3004–3014, https://doi.org/10.1016/j.ijhydene.2015.11.129.

[30] P. Hong, L. Xu, H. Jiang, J. Li, M. Ouyang, A new approach to online AC impedance measurement at high frequency of PEM fuel cell stack, Int. J. Hydrogen Energy 42 (30) (2017), https://doi.org/10.1016/j.ijhydene.2017.06.035, 19156–19169.

[31] B. Ratnakumar, M. Smart, L. Whitcanack, R. Ewell, The impedance characteristics of mars exploration rover li-ion batteries, J. Power Sources 159 (2) (2006) 1428–1439, https://doi.org/10.1016/j.jpowsour.2005.11.085.

[32] C. Jeppesen, S.S. Araya, S.L. Sahlin, S.J. Andreasen, S.K. Kr, An EIS alternative for impedance measurement of a high temperature PEM fuel cell stack based on current pulse injection, Int. J. Hydrogen Energy 42 (24) (2017) 15851–15860, https://doi.org/10.1016/j.ijhydene.2017.05.066.

[33] R. Isermann, M. Mnchhof, Identification of Dynamic Systems, Springer Berlin Heidelberg, 1985.

[34] N. Xiang, Using m-sequences for determining the impulse responses of LTI-systems, Signal Process. 28 (1992) 139–152, https://doi.org/10.1016/0165-1684(92)90031-Q.

[35] X. Yuan, J.C. Sun, H. Wang, J. Zhang, AC impedance diagnosis of a 500W PEM fuel cell stack: Part II: individual cell impedance, J. Power Sources 161 (2) (2006) 929–937, https://doi.org/10.1016/j.jpowsour.2006.07.020.

[36] M. Rhif, B. A. Ali, I. R. Farah, B. Martnez, Y. Sang, Wavelet transform application for/in non-stationary time-series analysis: a review, Appl. Sci. 9 (7). doi:10.3390/app9071345.

[37] Y. Hoshi, N. Yakabe, K. Isobe, T. Saito, I. Shitanda, M. Itagaki, Wavelet transformation to determine impedance spectra of lithium-ion rechargeable battery, J. Power Sources 315 (2016) 351–358, https://doi.org/10.1016/j.jpowsour.2016.03.048.

[38] I. Daubechies, Ten Lectures on Wavelets, Society for Industrial and Applied Mathematics, 1992.

[39] R.J. Baxley, B.T. Walkenhorst, G. Acosta-Marum, Complex Gaussian ratio distribution with applications for error rate calculation in fading channels with imperfect CSI, in: 2010 IEEE Global Telecommunications Conference GLOBECOM 2010, IEEE, Miami, FL, USA, 2010, pp. 1–5, https://doi.org/10.1109/GLOCOM.2010.5683407.

[40] J.E.B. Randles, Kinetics of rapid electrode reactions, Discuss. Faraday Soc. 1 (4) (1947) 11–19.

[41] P. Pathapati, X. Xue, J. Tang, A new dynamic model for predicting transient phenomena in a PEM fuel cell system, Renew. Energy 30 (1) (2005) 1–22, https://doi.org/10.1016/j.renene.2004.05.001.

[42] A. Fitzgibbon, M. Pilu, R.B. Fisher, Direct least square fitting of ellipses, IEEE Trans. Pattern Anal. Mach. Intell. 21 (5) (1999) 476–480, https://doi.org/10.1149/1.217920010.1109/34.765658.

[43] Z. Li, R. Outbib, S. Giurgea, D. Hissel, Diagnosis for PEMFC systems: a data-driven approach with the capabilities of online adaptation and novel fault detection, IEEE Trans. Ind. Electron. 62 (8) (2015) 5164–5174, https://doi.org/10.1109/TIE.2015.2418324.

[44] Y. Ma, G. Guo, Support Vector Machines Applications, Springer Berlin Heidelberg, 2014.

[45] B. Fei, J. Liu, Binary tree of SVM: a new fast multiclass training and classification algorithm, IEEE Trans. Neural Netw. 17 (3) (2006) 696–704, https://doi.org/10.1109/TNN.2006.872343.